Ceramics International 51 (2025) 11363–11371

Contents lists available at ScienceDirect

Ceramics International

journal homepage: www.elsevier.com/locate/ceramint

Interactions of sulfur-containing gas with magnesia-chromite refractory in nickel flash smelting furnace

Juho Lehmusto [a,*], Saara Söyrinki [b], Juha Lagerbom [b], Tuomas Jokiaho [b], Zaiqing Que [b], Jorma Määttä [c], Leena Hupa [a], Elina Huttunen-Saarivirta [b], Mari Lindgren [d]

[a] Faculty of Science and Engineering, Abo Akademi University, Turku, Finland
[b] VTT Technical Research Centre of Finland Ltd, Espoo, Finland
[c] Institute of Biomedicine, University of Turku, Turku, Finland
[d] Metso, Pori, Finland

ARTICLE INFO

Handling Editor: Dr P. Vincenzini

ABSTRACT

As-received and spent magnesia-chromite refractories from a nickel flash smelting furnace were analyzed and compared to shed light on the interactions between the gas phase and the refractory material, a topic that has not received previous research effort. Based on the results, process-originated gaseous sulfur-containing species, such as SO_2 and SO_3, played a key role in the refractory reactions. In the absence of a surface deposit, the hot end of the refractory underwent attack by SO_2, resulting in sulfation of both the periclase and chromite phases, which has not been reported before. In the presence of a surface deposit, the sulfation of main phases in the near-surface regions did not occur, but sulfur-bearing species diffused deeper into the refractory material, where they reacted with MgO and CaO, forming $MgSO_4$ and $CaSO_4$. In addition to the detected sulfur penetration, impurity elements, e.g., As; K, and Pb, had diffused towards the cold end of the refractory. This suggests these elements could have entered the refractory as gaseous species and then condensed at low enough temperatures.

1. Introduction

A flash smelting process is one of the key technologies in sustainable copper and nickel production. In the flash smelting process, finely ground concentrates of sulfide-rich ores are mixed with oxygen-enriched air and ignited. Combustion of the feed releases enough energy to keep the smelting of the supplied concentrate ongoing. As a result, the process is self-sustaining and requires no external fuel, enabling low total energy consumption and carbon dioxide emissions by a flash smelter plant despite the high temperatures of pyrometallurgy [1]. In such a process, the sulfur-rich gas atmosphere may reach temperatures up to 1400 °C. Therefore, refractory materials with well-known and optimized properties are required to protect the interior of the flash smelting furnace.

Magnesia-chromite spinel-based refractories are utilized in copper and nickel flash smelting furnaces due to their excellent durability against heat, thermal shocks, and melt erosion forces as well as high resistance against slags with different basicities [2–4]. The studied material belongs to the magnesia-chromite refractory family, which relies on the use of chromite ore, $FeCr_2O_4$, added with magnesia and processed along different routes into ceramics of diverse bonding types, compositions, and purity levels [5]. Despite the good properties of magnesia-chromite refractories, they are not entirely inert to the flash smelter environment. For example, acidic slags react with the periclase (MgO) phase in the refractory, resulting in material degradation [1]. In addition to the contact with slag, refractories in the gas zone are subjected to an aggressive gaseous atmosphere rich in SO_2 that forms upon oxidation of the sulfur in the ore. The increased use of recycled material streams may further introduce new reactive impurities, such as halides, lead, and zinc, to the process gas. Although optimized microstructurally due to heat conductivity reasons, refractory ceramics always involve porosity that enables the transport of gaseous species. Indeed, lead and zinc have been found inside a refractory brick used in a submerged arc furnace [6]. Furthermore, thermal gradients develop across the refractory lining between the hot gaseous atmosphere in the interior of the flash smelting furnace and the cooled internal walls of the furnace. These may pose an additional factor that contributes to the transport of

* Corresponding author.
E-mail addresses: juho.lehmusto@abo.fi (J. Lehmusto), Saara.Soyrinki@vtt.fi (S. Söyrinki), Juha.Lagerbom@vtt.fi (J. Lagerbom), Tuomas.Jokiaho@vtt.fi (T. Jokiaho), Zaiqing.Que@vtt.fi (Z. Que), jmaatta@utu.fi (J. Määttä), leena.hupa@abo.fi (L. Hupa), Elina.Huttunen-Saarivirta@vtt.fi (E. Huttunen-Saarivirta), mari.lindgren@metso.com (M. Lindgren).

https://doi.org/10.1016/j.ceramint.2024.12.555
Received 31 October 2024; Received in revised form 19 December 2024; Accepted 31 December 2024
Available online 3 January 2025

species within the refractory and, hence, to the reactions that may occur between components of the gas atmosphere and the refractory.

The SO_2 content in the flash smelting furnace atmosphere is high, varying from 20 to 70 vol% [7,8]. Such conditions may lead to interactions between SO_2 and the refractory lining, resulting in refractory degradation. Additionally, SO_2 may react with the available oxygen, O_2, introducing SO_3 according to Ref. [9]:

$$2SO_{2(g)} + O_{2(g)} \rightarrow 2SO_{3(g)} \quad \text{(Equation 1)}$$

In such cases, the reactive SO_3 diffuses in the refractory through the pores and easily reacts with the spinel phase according to Equations (2) and (3) [10]:

$$MgCr_2O_{4(s)} + SO_{3(g)} \rightarrow MgSO_{4(s)} + Cr_2O_{3(s)} \quad \text{(Equation 2)}$$

$$MgFe_2O_{4(s)} + SO_{3(g)} \rightarrow MgSO_{4(s)} + Fe_2O_{3(s)} \quad \text{(Equation 3)}$$

A corresponding reaction has been identified in the periclase phase within the magnesia-chromite refractory, particularly in the cooler regions of the converter lining, resulting in the development of magnesium sulfate, $MgSO_4$, in accordance with Equation (4) [11]:

$$MgO_{(s)} + 0.5O_{2(g)} + SO_{2(g)} \rightarrow MgSO_{4(s)} \quad \text{(Equation 4)}$$

Also, CaO, present in the refractory as an impurity can react analogously to Equation (4), forming $CaSO_4$ following [12,13]:

$$CaO_{(s)} + 0.5O_{2(g)} + SO_{2(g)} \rightarrow CaSO_{4(s)} \quad \text{(Equation 5)}$$

The spinel dissociation following Equations (2) and (3) and the formation of trivalent oxides of Cr, Fe, and, possibly, Al in the structure challenge the microstructural integrity and promote wear of the refractory. Furthermore, the formation of $MgSO_4$ (Equation (4)) results in a four-fold increase in molar volume in comparison to the original periclase phase, MgO, resulting in refractory internal cracking and easy peeling off [10].

Despite the above-described fundamental research on the reactions between the flash smelting gaseous environment and the phases in the magnesia-chromite refractories, the aging of refractories in nickel flash smelting furnaces is rarely addressed in the literature. Indeed, most existing studies on the degradation of refractory ceramics in pyrometallurgy processes focus on slag contact, especially in the copper converters, so information about the reactivity and reaction mechanisms of the gas-zone refractories in flash-smelting furnaces is even more scarce. Because of this, very little is known about the refractory degradation in the gas zone. This paper bridges this knowledge gap by presenting unique results on the refractory degradation in the gas zone of the nickel flash smelter. Another feature, whose effect on refractory microstructure and degradation is unknown, is the significant temperature gradient over the refractory material in the furnace; this paper is unique also in addressing the contribution of the thermal gradient to the refractory degradation. Additionally, as impurities from raw materials may enter the refractory structure due to a thermal gradient, the results are expected to contribute to the recycling of spent refractories. Therefore, knowing which elements and their possible concentrations provides a means to deal with them safely.

In this work, unused refractories and corresponding spent refractories sampled from a nickel flash-smelting furnace were analyzed and compared to shed light on the interactions between the sulfur-rich gas phase and the refractory material. Special attention was paid to defining the role of sulfur species in changes in the refractory composition, microstructure, and morphology. This information is essential for understanding the transport of sulfur species following thermal gradients across the refractory lining during furnace operation. Nickel flash smelting operates inherently at higher temperatures compared to copper flash smelting and this is expected to play a key role in how the microstructure and composition of the refractory evolve in use. The results lay the basis for designing controlled lab-scale experiments, computational modeling of refractory behavior, and deriving strategies for mitigating the degradation.

2. Experimental

2.1. Materials

Refractory brick RADEX OX6 by RHI Magnesita was examined in this research. The brick was a magnesia-chromite product of type MCr50, ISO 10081-2. According to the manufacturer, the composition of the brick is as follows (in wt.%): 59.5 MgO, 19.0 Cr_2O_3, 13.5 Fe_2O_3, 6.0 Al_2O_3, 1.3 CaO, and 0.5 SiO_2, with the apparent porosity of 17.0 vol%. The material was investigated both in as-received and spent conditions. All spent bricks had served under conditions with a gas atmosphere containing about 50 vol% SO_2 at 1400 °C and dust particles consisting of mainly partially oxidized nickel concentrate and silica flux. The typical campaign time is 10 years [1]. The individual spent bricks were selected for investigation to include both the bricks that were covered by a deposit and the ones without the deposit, i.e., exposed directly to the sulfur-bearing gas phase. To facilitate the understanding of the role of thermal gradient, the orientation of spent refractories with respect to the internal part of the smelter and the cooled external walls was recorded.

The as-received bricks were dry-cut using a diamond saw to avoid loss of water-soluble species. The cut specimens were subjected to mercury porosimetry and μ-computed tomography (μ-CT) without further sample preparation procedures. X-ray diffraction (XRD) measurements were conducted for gently ground specimens. For the examinations by light microscopy (LM) and field-emission gun scanning electron microscopy studies (FEG-SEM), the specimens were further cast into resin, ground, and suspension-polished down to below 1 μm surface finish. Two different SEMs were used: a Zeiss Crossbeam 540 equipped with an EDAX Hikari Plus (EBSD) detector and a Thermo Scientific Apreo S high-resolution microscope, 164 coupled with an Oxford Instruments Ultim Max 100energy dispersive X-ray spectroscope. Both SEMs were operated with an accelerating voltage of 20 kV.

2.2. Methods

In the case of spent refractories, the loose deposit that covered the refractory surface facing the smelter was analyzed by scraping it off with a surgical blade for powder XRD analyses. Additionally, samples were drilled from the bulk of the spent refractory, gently ground, and then subjected to XRD measurements. Towards the cold end, white powder covering the brick was also scraped with a surgical blade and collected for powder XRD analyses. Selected areas of the brick were also subjected to μ-XRF measurements. For microscopy studies, the bricks were cast into resin to hold the cracked structure together and cut into 1–2 cm thick slices to enable closer examination of possibly altered microstructure and chemical composition. The resin-embedded slices were further platinum-coated to enable FEG-SEM examinations. XRD measurements were performed using a Panalytical Empyrean X-ray diffractometer. It was operated with monochromated CuK_α radiation at 45 kV/40 mA. Philips X'Pert HighScore program equipped with a Powder Diffraction File (PDF) database was used for the phase identification and comparison.

FEG-SEM imaging was executed in a back-scattered electron (BSE) mode. The associated elemental mapping was performed with acceleration voltages of 15 and 20 kV, WD of 15 mm, and a probe current of 3 nA.

Pore size distributions were determined by mercury intrusion porosimetry using Pascal 140 and Pascal 440, Thermo Electron S.P.A., Milan, Italy. Porosimetry was used with a maximum test pressure of 400 MPa (corresponding to a minimum Laplace throat diameter of 3.7 nm) at 24 °C. Corrections for the compression of mercury, glassware, and oil phase were taken into account by running a blank experiment.

Micro-computed tomography (μ-CT) was performed with a Bruker-

Skyscan 1272 X-ray computer tomography scanner (Bruker, Madison, WI, USA) equipped with a Hamamatsu L10101 16-megapixel camera. Reconstruction of the cross-sectional images was done with InstaRecon 2.4.0.5 software and data analysis and 3D model building with CTan 1.19.10.2 software, both from Skyscan (Bruker, Madison, WI, USA). Three different density subsets were visually apparent in the as-received refractory. False-color models were rendered from reconstituted image stacks by the CTvox 3.3.0 program (Skyscan).

μ-XRF mapping of the samples was conducted using a Bruker M4 TORNADO spectrometer equipped with two silicon drift detectors, an Rh X-ray source, and a polycapillary lens. The spot of ~20 μm and a 30-ms pixel time were used for scanning in a 20-mbar vacuum. The tube voltage was 50 kV, and the current was 600 μA. Before the measurements, both spectrometers were calibrated using a Zr standard.

3. Results and discussion

In the presentation and discussion of results for the spent refractories, the main division between the individual bricks is based on whether the surface facing towards the internal part of the smelter contains a surface deposit or if it is deposit-free. Further, the characterized zones of the spent refractories are referred to as the "hot end" and "cold end", based on whether they have faced the hot internal part of the smelter or cooled external walls of the furnace (Fig. 1).

3.1. As-received refractory material

XRD analyses, Fig. 2a, disclosed the presence of two phases in the as-received refractory material: periclase, MgO (67 %), and chromite (Mg,Fe)(Cr,Al)$_2O_4$ identified by XRD as picotite, $MgCr_2O_4$ (33 %). The chromite phase can be further divided into primary and secondary chromite with slightly different chemical compositions (Table 1). Primary chromite is present in the refractories as individual grains embedded in the periclase phase, whereas secondary chromite fills the intergranular areas. The periclase phase includes relatively much lower amounts of dissolved metals, Cr, Fe, and Al. Based on cross-sectional SEM images (Fig. 3), the periclase phase (areas with the dark grey contrast in Fig. 3) forms the matrix for the chromite aggregates (areas with the light grey contrast in Fig. 3), in addition to which pores with varying sizes are present throughout the structure. The measured porosity of 16 vol%, bulk density of 3.44 g cm^{-3}, and phase densities agreed well with previously reported values (MgO (3.58 g cm^{-3}), $MgCr_2O_4$ (4.41 g cm^{-3}), and $MgFe_2O_4$ (4.45 g cm^{-3})) [9,14–16].

Fig. 1. A photomacrograph of a brick sample from the gas-zone roof lining close to the uptake shaft of a nickel flash smelting furnace. This spent refractory sample contains the deposit.

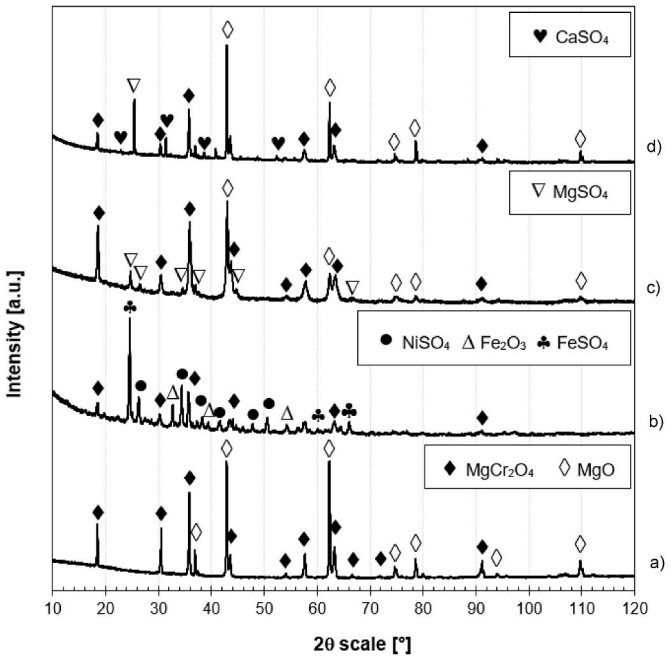

Fig. 2. XRD patterns for a) as-received and b-d) spent refractory. Spent refractory was analyzed in areas representing b) hot end with the deposit, c) hot end without the deposit, and d) cold end. The following PDF numbers were used for the identified phases: $MgCr_2O_4$: 04-016-2691; MgO: 04-004-8990; $NiSO_4$: 04-017-6385; Fe_2O_3: 04-006-0285; $FeSO_4$: 00-017-0873; $MgSO_4$: 04-015-4049; $CaSO_4$: 04-007-4744.

Table 1
Compositions of the phases in as-received material determined by EDS (in wt.%).

	O	Mg	Al	Cr	Fe
MgO	34.7	59.6	0.5	2.3	3.9
	32.4	13.9	8.2	32.9	12.2
(Mg,Fe)(Cr,Al)$_2O_4$ (Primary)					
	32.4	14.7	7.4	27.9	17.7
(Mg,Fe)(Cr,Al)$_2O_4$ (Secondary)					

Furthermore, the pore size distribution (Median pore diameter 18.9 μm with 61 % of the pores having a diameter between 11 and 30 μm) agreed fairly well with the values reported earlier [14]. Calcium was detected between the periclase grains, most likely as (Ca,Mg)$_2SiO_4$ or dissolved in Mg_2SiO_4 [17]. In addition to the evident porosity of the microstructure, it contained microcracks that may propagate through the phase boundary due to the close orientation relationship between the phases.

3.2. Refractory material from the flash smelting furnace, hot end

In two of the studied spent refractories, a deposit covered the hot end surface. As revealed by XRD investigations, Fig. 2b, the deposit grown on the refractory contained Fe_2O_3. $FeSO_4$, and $NiSO_4$, in addition to the refractory components. Oxides of nickel and iron are common constituents in the flue dust that forms in the nickel smelter and is carried by the gas flow [18,19]. Typically iron oxide is present as Fe_3O_4, but the oxidation had most likely continued in the loose deposit layer during cooling, forming Fe_2O_3 along with $FeSO_4$ and $NiSO_4$ that developed upon sulfation of the dust [18]. It should, however, be noted that sulfates of nickel and iron are not stable in the operating temperatures (up to 1400 °C) but exist as oxide compounds in SO_2 rich atmosphere that then form sulfates upon cooling down to 810 °C ($NiSO_4$) [20], 625 °C ($Fe_2(SO_4)_3$), or 525 °C ($FeSO_4$) [21].

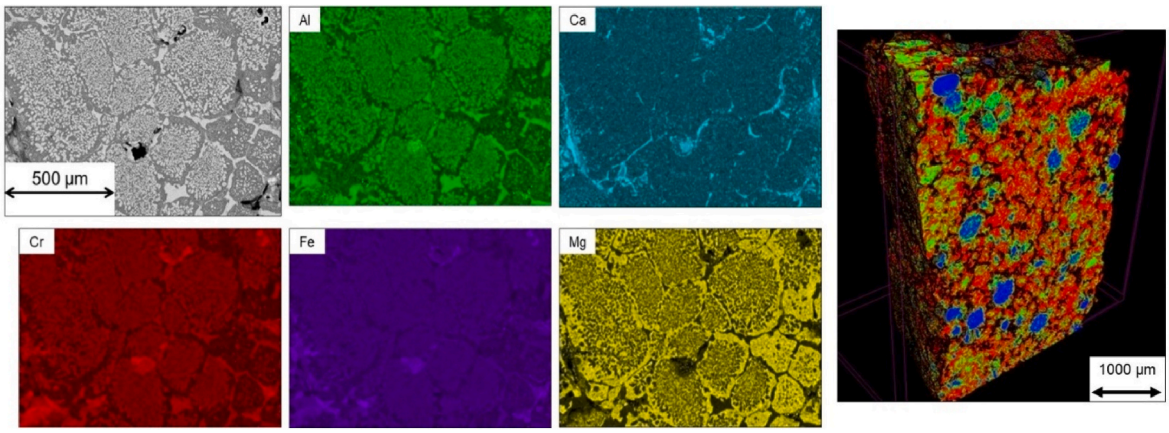

Fig. 3. Elemental composition and three-dimensional density distribution of the as-received material. In the density map, areas with low density are red, medium density are green, and high density are blue. The black regions are pores. (For interpretation of the references to color in this figure legend, the reader is referred to the Web version of this article.)

The panoramic SEM image in Fig. 4 shows the microstructure of the spent refractory at the outermost part of the brick in a sample that was covered with a deposit. Compared to the as-received material, the inherent morphology of the spent refractory was essentially denser. The dense structure of the material implies that it has likely melted or at least undergone profound solid-state diffusion. Although sintering of a pure $MgCr_2O_4$ phase requires as high temperatures as 1700 °C [22], soluble oxides, such as Fe_2O_3, can decrease the corresponding temperature for $MgCr_2O_4$ well below 1400 °C [22], as observed in the present work. The densified refractory structure, observed also earlier in

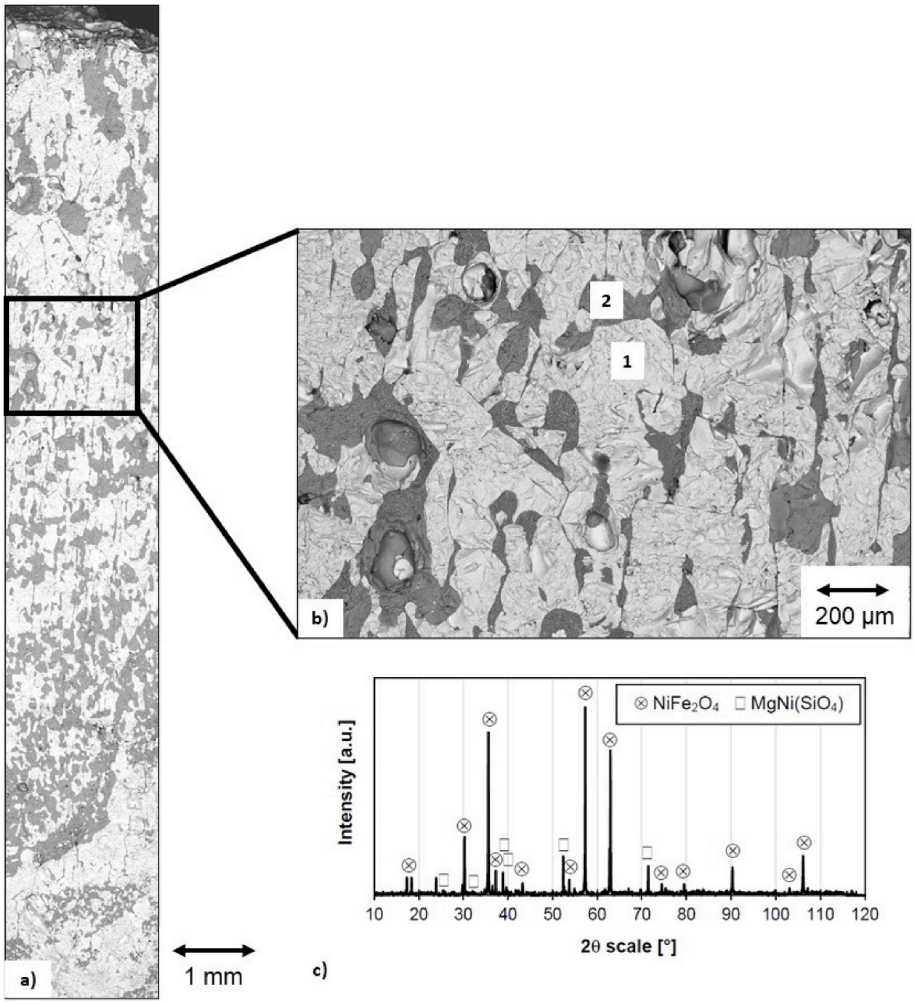

Fig. 4. Panoramic SEM image showing the microstructure of a spent refractory from the roof lining before the uptake shaft (a,b). The panorama is taken from the refractory surface to a depth of 10 mm. The gas zone is located at the top. XRD pattern for the identified phases (c). The following PDF numbers were used for the identification: $NiFe_2O_4$: 01-081-8428; $MgNi(SiO_4)$: 04-013-9259.

magnesia-chromite refractories [23], may also form when slag infiltrates the structure and subsequently fills the pores. Nonetheless, two types of regions were still recognizable in the dense refractory structure; a light grey phase, marked with "1" in Fig. 4 and a dark grey phase, marked with "2" in Fig. 4. The chemical composition of both phases differed from the initial ones; Area 1 contained relatively much higher amounts of Fe and Ni than the primary or secondary chromite phases in the as-received material, whereas Si and Ni were enriched in Area 2 (Table 2). Furthermore, the amounts of Cr and Al included in both phases were virtually lowered to 0 %. Two phases could by identified by XRD: $NiFe_2O_4$ and $MgNi(SiO_4)$.The presence of Ni in almost equal quantities in both phases suggests that it has infiltrated the refractory material as melt or desposited from the dust rather than specifically reacted with one of the phases. The fact that Ni could not be identified deeper in the material relates to the presence of a thermal gradient along the brick, hence the temperature had decreased to a low enough level to solidify Ni. The high Fe concentration in Area 1 can be explained by the gradual replacement of Cr^{3+}/Al^{3+} ions with the inward-diffused Fe^{3+} ions from the feed material [2]. Such incorporation of species from the feed material into the refractory may result in the precipitation of multicomponent spinels [30]. With AB_2O_4 -type spinels, such as picotite, the replacement of ions in the original structure can occur by incorporated ions with an appropriate ionic radius (e.g., Fe^{2+}, Ni^{2+}, Cu^{2+}, Zn^{2+}) [31]. In addition to the compositional changes of the refractory matrix due to the infiltration of elements from the feed material, the structural densification most likely affects properties, such as phase volume and thermal conductivity. This may lead to refractory cracking during cooling of the furnace in a maintenance shutdown.

In area 2, the incorporation of Si from the slag was evident. XRD analyses revealed the presence of $MgNi(SiO_4)$, reflecting that the slag had reacted with the magnesium-bearing constitutents of the refractory. However, XRD analyses did not disclose a direct reaction between the slag and the MgO in the refractory into a forsterite phase ($2MgO{\cdot}SiO_2$) according to Equation (6) [24–27]. Such a forsterite phase has been earlier identified in used refractories from non-ferrous metals smelters such as copper [28]. It forms mainly between magnesia and chromite grains, causing the swelling of the microstructure, and through that, results in cracking of the refractory [29].

$$2MgO_{(refractory)} + SiO_{2(slag)} \rightarrow Mg_2SiO_{4(solid\ solution)} \quad \text{(Equation 6)}$$

One explanation for the absence of the forsterite phase could be the preferential reaction of the slag with the picotite phase, $MgCr_2O_4$.

In the absence of a visible surface deposit, the behavior of the refractory changed. XRD studies, Fig. 2c, revealed the presence of $MgSO_4$ along with the original refractory phases. In agreement with this, EDS analyses on the hot end of the spent refractory (Table 3) disclosed that sulfur had penetrated the structure (Fig. 5, areas 6, 7, 8, and 9). Interestingly, both main phases occasionally contained high concentrations of sulfur. The periclase phase, seen in dark grey contrast in the SEM BSE image (Fig. 5, areas 8 and 9) contained up to 17 wt% sulfur at its highest, suggesting the evolution of $MgSO_4$. Sulfur could also be found in larger primary chromite grains (Fig. 5, areas 6 and 7), manifested as enrichment in S and depletion in Cr and Fe in comparison to original phase compositions (Table 1), suggesting sulfation of the $(Mg,Fe)(Cr,Al)_2O_4$ phase and also resulting in $MgSO_4$ formation.

If the chromite phase $(Mg,Fe)(Cr,Al)_2O_4$ in the as-received material is divided into binary spinels $MgFe_2O_4$, $MgCr_2O_4$, and $MgAl_2O_4$, the reactivities of these spinels can be compared. It should be mentioned that the spinel structure can undergo temperature-dependent structural changes, in other words, reversible phase transitions, which affect the reactivity of the structure. For the three above-mentioned spinels, structural inversion takes place within the following temperature ranges: 1176–1346 °C for $MgAl_2O_4$ in the heating cycle and 1449–1205 °C in the cooling cycle; 1186–1356 °C for $MgCr_2O_4$ in the heating cycle and 1366–1226 °C in the cooling cycle; and 1036–1356 °C for $MgFe_2O_4$ in the heating cycle [32]. Even though all three spinels undergo structural changes at temperatures prevailing inside the refractory brick, $MgFe_2O_4$ is reported to have the highest reactivity with SO_3, forming $MgSO_4$ and Fe_2O_3 [33]. Depending on the SO_3 partial pressure, $MgSO_4$ is stable in the temperature range of 300–1000 °C, $Cr_2(SO_4)_3$ is stable until reaching a temperature between 707 °C and 727 °C, whereas $Fe_2(SO_4)_3$ and $Al_2(SO_4)_3$ are stable up to 657 °C [34].

Table 2
Elemental compositions of the phases marked in Fig. 4.

Element	Area 1		Area 2	
	Wt%	At%	Wt%	At%
O	25.3	53.1	37.7	55.5
Mg	2.6	3.6	20.9	20.2
Si	0.4	0.5	17.4	14.6
Ca	0.0	0.0	0.2	0.1
Fe	52.9	31.8	2.5	1.1
Al	0.5	0.6	0.0	0.0
Ni	17.4	10.0	19.6	7.9
Cu	0.9	0.5	0.9	0.3
Co	0.0	0.0	0.7	0.3

Table 3
Elemental compositions of the areas marked in Fig. 5.

	O	Mg	Al	S	Ca	Ti	V	Cr	Fe
1	32.8	31.8	3.5	5.4	0.5	0.3	–	13.7	12.0
2	32.0	43.3	1.9	2.7	–	–	–	10.6	9.6
3	32.2	49.8	1.5	1.6	–	–	–	5.0	9.9
4	30.5	14.4	8.2	0.9	0.3	0.5	–	37.8	7.4
5	30.6	14.0	7.8	0.9	0.3	0.4	0.3	36.0	9.7
6	36.0	18.2	3.7	12.1	0.6	0.3	–	23.0	6.0
7	38.2	18.7	3.5	13.4	0.5	0.3	–	21.4	4.0
8	39.0	36.8	0.9	11.2	1.0	–	0.2	3.7	7.3
9	43.2	30.4	0.6	17.1	0.2	–	–	2.5	6.0
10	31.9	15.4	10.8	1.4	–	–	–	37.8	2.8
11	34.2	17.9	7.6	7.0	0.2	–	0.2	29.6	3.3

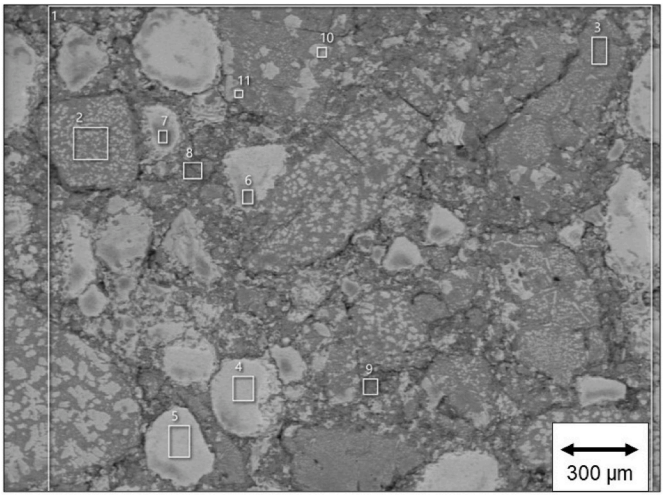

Fig. 5. A cross-sectional SEM image of the hotter part of the spent refractory. The gas zone is located towards the top of the image.

This makes $MgSO_4$ the most stable sulfate compound in the temperature range through the studied refractories, explaining the presence of $MgSO_4$ in the spent refractory bricks addressed in this study.

3.3. Refractory material from the flash smelting furnace, cold end

Deeper in the spent refractory, calcium and sulfur were detected more frequently and at significantly higher amounts than in the hot end of the refractory. XRD analyses identified $CaSO_4$ and $MgSO_4$ in addition to the initial phases MgO and $MgCr_2O_4$, Fig. 2d. Based on the EDS maps (Fig. 6), it is evident that most of the pores in the structure were occupied by $CaSO_4$. Sulfur was also detected uniformly distributed in the structure, e.g., among the initial phases, which likely explains the observation of $MgSO_4$ in XRD patterns. Indeed, the coexistence of $MgSO_4$ with MgO and $MgCr_2O_4$ explains the detected high sulfur content in the magnesium-containing areas. Earlier, $CaSO_4$ has been identified both in spent refractories in copper smelting [2,13] and magnesia-based refractories exposed in laboratory studies to SO_2/SO_3 rich atmospheres at elevated temperatures [35], in particular filling the pores that existed in the refractory [2,24]. Therefore, the observations of this work are parallel to those reported in the literature.

The detection of $CaSO_4$ and $MgSO_4$ and the overall high sulfur content imply the enhanced transport of SO_2 deep inside the refractory brick, likely towards the cooled external surface. The results do not reveal whether the gaseous sulfur oxide transported into the refractory was in the form of SO_2 or as a more reactive SO_3. According to the literature [24], SO_2 is the dominant sulfur oxide form above the temperature of 760 °C, while SO_3 primarily exists at lower temperatures. Thus, the SO_2-to-SO_3 conversion is temperature-dependent and driven by cooling to temperatures lower than 760 °C. It is also possible that the deposit at the refractory surface, or the refractory itself, catalyzes the conversion. The process dust of a nickel flash smelting furnace has previously been shown to catalyze the SO_2-to-SO_3 conversion [36]. In any case, the likely reactions with CaO and MgO within the refractory in the presence of SO_3 are [37,38]:

$$CaO_{(s)} + SO_{3(g)} \rightarrow CaSO_{4(s)} \quad \text{(Equation 7)}$$

$$MgO_{(s)} + SO_{3(g)} \rightarrow MgSO_{4(s)} \quad \text{(Equation 8)}$$

Regarding Equations (7) and (8), it has been reported that MgO indicated higher reactivity than CaO at temperatures above 650 °C [39,40]. Furthermore, CaO reacts more readilywith SO_3 (Eq. (8)) than with SO_2 (Eq. (5)), hence $CaSO_4$ can be expected particularly in the cooler parts of the refractory where SO_3 formation is preferred [37]. The initial CaO concentration in the refractory was 1.3–1.5 %. Therefore, the solid-state diffusion of Ca^{2+} ions, mainly through the crystal defects (vacancies, dislocations, and grain boundaries), could explain the presence of $CaSO_4$ primarily in the cold end of the refractory [41–43].

According to the literature [41], the immediate effect of the build-up of $CaSO_4$ is the increase of the internal volume: the molar volume of $CaSO_4$ is roughly three times the molar volume of CaO that was detected in the as-received refractory material. However, no extensive microcracking was seen close to the $CaSO_4$-rich areas.

3.4. Implications to refractory wear

During operation, the refractories are exposed to demanding conditions of high temperatures and sulfur-rich atmospheres with feed mixture constituents that undergo reactions. The interactions between magnesia-chromite refractories and the slags have been studied extensively, e.g., Refs. [2,6,11,17,23,44–46]. However, most applications considered, such as converters, involve gaseous atmospheres, which are much milder in terms of their corrosivity than the flash smelting furnaces. The present work focuses on the interactions between the refractory, sulfur-rich furnace atmosphere and temperature gradient; a topic not covered by earlier research. A substantial thermal gradient forms between the gas temperature of about 1400 °C and the cold end along a refractory brick with a thickness of approximately 250 mm.

To confirm the role of thermal gradient in the reactions in the refractory, μ-XRF analyses were conducted over the brick length.

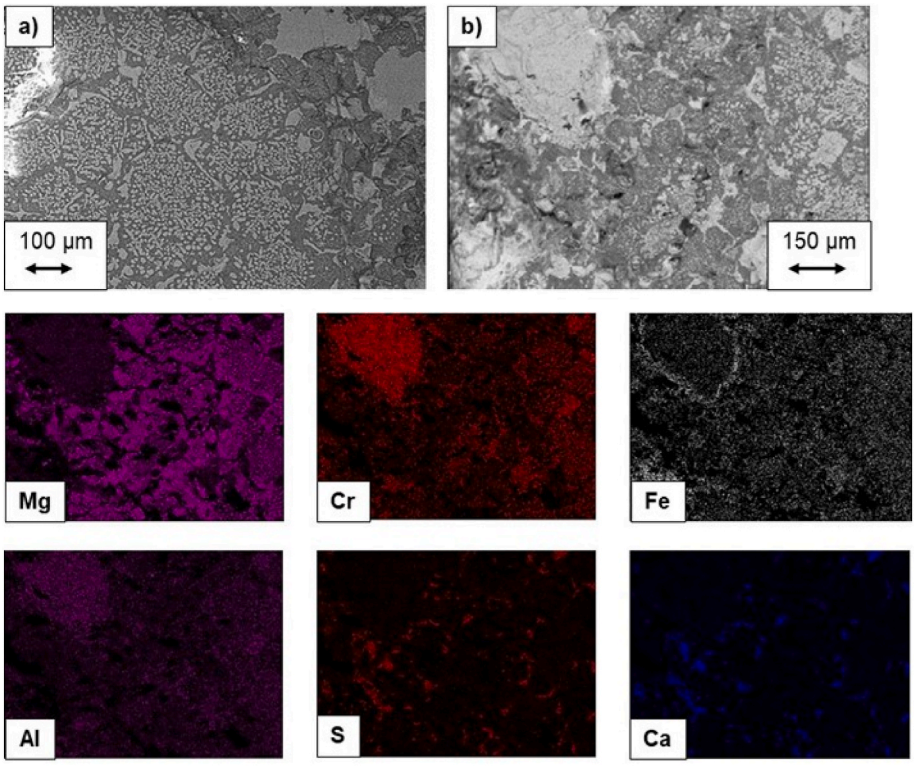

Fig. 6. SEM images (a, b) and EDS maps for the reacted cold-end refractory from the roof lining before the uptake shaft.

According to μ-XRF analyses, the deposit at the gas/refractory interface consisted mainly of Fe, Ni, and Si with Cu and As (Fig. 7). These findings are consistent with the XRD and SEM observations, with the addition of the detection of As. Furthermore, μ-XRF investigations revealed that As, K, Pb, and S had diffused towards the cool end of the refractory in the sample taken from the smelter roof (Fig. 8), yet these elements had different concentration profiles. Only the concentration of S increased towards the cool end of the refractory. This suggests that the diffusion was essentially driven by a thermal gradient. Conversely, although diffused deep in the refractory, the concentrations of As, K, and Pb showed a steadily decreasing trend towards the cool end of the material. Overall, these profiles indicate that the porosity in the refractory brick is high enough for (specific) gaseous species to diffuse into the material, which is a prerequisite for their contribution to reactions with the refractory constituents. It is emphasized that the reason why EDS did not identify all named elements is the higher sensitivity of μ-XRF, allowing it to detect lower amounts of elements.

Comparing the samples with and without the deposit on the refractory showed clearly its beneficial effect. In the refractory without the deposit, the hot end of the refractory had experienced sulfation of its main phases. This has led to the significant deterioration of the microstructure and complete loss of the mechanical integrity effectively limiting the lifetime of the material. The fact that this phenomenon was only seen in the hot end may explain why this has not been detected in copper smelters where the temperature is inherently somewhat lower.

The presence of a deposit on the refractory surface has been sufficient to prevent the sulfation of the main phases, possibly due to its insulating effect. In this case, the sulfurous gases have penetrated deeper into the refractory material and reacted with the minor phase or to a very small extent with the MgO phase. The reactions have occurred at the cold end of the refractory, presumably because of the SO_3 formation tendency at lower temperatures. At the same time, the hot end of the refractory had densified as a result of the infiltration of Ni, Si, and Fe from the process. These changes have, however, had only a minor influence on the refractory integrity. This clearly demonstrates the beneficial effect of deposit formation on the refractories.

The results revealed that impurities from the raw materials, like As and Pb, enter the refractory. Although the contents are very low, as they can only be detected by the very precise methods, like μ-XRF, it is clear

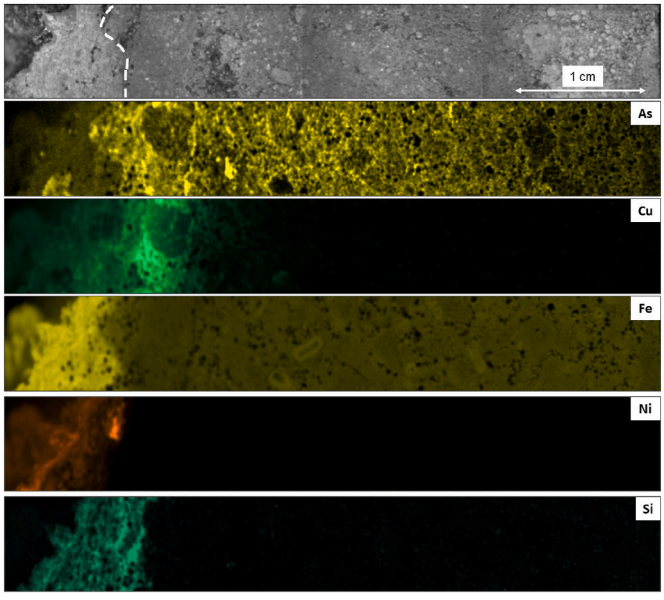

Fig. 7. μ-XRF maps showing the chemical composition of the deposit and the sub-surface region of a refractory brick from the roof lining of a nickel flash smelting furnace. The rough interface between the deposit and the refractory is marked with a white dashed line. The real-life length of the image is 5 cm.

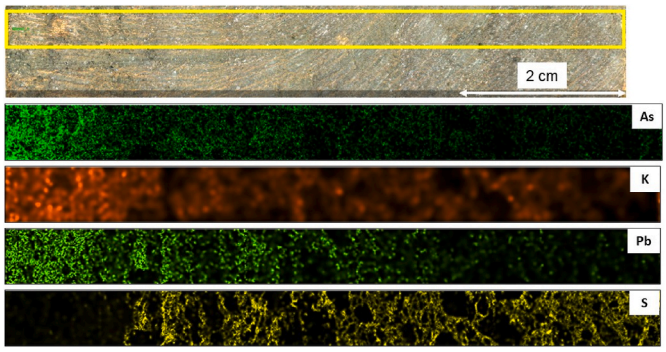

Fig. 8. μ-XRF maps showing the effect of the temperature gradient on diffusion in a refractory brick from the roof lining of a nickel flash smelting furnace. The cool end of the sample is to the right.

that their presence should be taken into account while recycling the refractories. For example, it should be taken care that the heavy metals are not leached out in the nature and are handled following the work safety guidelines.

4. Conclusions

Based on the comparison of the phase compositions and microstructures of an unused magnesia-chromite refractory and the same material received from an operational nickel smelting furnace after several years of use, the following conclusions addressing phase stability and refractory wear were drawn:

i) The as-received magnesia-chromite refractory has a two-phase microstructure of MgO and $MgCr_2O_4$, with evident porosity and microcracks that may propagate through the phase boundary due to the close orientation relationship between the phases.
ii) In the absence of a surface deposit, the outermost parts of the refractory are prone to be attacked by the sulfur-bearing smelter atmosphere, resulting in the sulfation of both of the main phases.
iii) In the presence of a surface deposit in the hot end of the refractory, sulfur-bearing species diffuse deeper into the refractory material, where they primarily react with MgO and CaO, forming $MgSO_4$ and $CaSO_4$.
iv) In addition to the sulfur penetration, process-related elements such as Fe, Ni, and Si impregnated the refractory, leading to structural and chemical changes in the matrix. This may alter the physical properties of the refractory, leading to mechanical degradation (cracking) during cooling.
v) Thermal gradient across the refractory explains its reactions with the furnace atmosphere, particularly with SO_3, whose contribution is favored by temperatures lower than 760 °C.
vi) In addition to sulfur, the diffusion behavior of several impurities, such as As, K, and Pb stems from the temperature gradient. Although the detrimental effect of these impurities could not be verified, their role might become relevant in the future with increasing sidestream volumes in the flash smelting process.
vii) Regarding practical applications, the presence of a dense deposit or a phase at the refractory surface is beneficial in terms of slowing down sulfur penetration, and through that, the deterioration of the refractory microstructure.

CRediT authorship contribution statement

Juho Lehmusto: Writing – original draft, Methodology, Investigation, Funding acquisition, Formal analysis, Conceptualization. **Saara Söyrinki:** Writing – review & editing, Methodology, Investigation, Formal analysis. **Juha Lagerbom:** Writing – review & editing,

Methodology, Investigation. **Tuomas Jokiaho:** Methodology, Investigation. **Zaiqing Que:** Writing – review & editing, Methodology, Investigation. **Jorma Määttä:** Writing – review & editing, Methodology, Investigation. **Leena Hupa:** Writing – review & editing, Supervision, Funding acquisition. **Elina Huttunen-Saarivirta:** Writing – original draft, Supervision, Methodology, Investigation, Funding acquisition, Formal analysis, Conceptualization. **Mari Lindgren:** Writing – original draft, Supervision, Methodology, Investigation, Funding acquisition, Formal analysis, Conceptualization.

Declaration of competing interest

The authors declare the following financial interests/personal relationships which may be considered as potential competing interests: Juho Lehmusto reports financial support was provided by Research Council of Finland. Juho Lehmusto reports financial support was provided by Business Finland. Saara Soyrinki reports financial support was provided by Business Finland. Juha Lagerbom reports was provided by Business Finland. Tuomas Jokiaho reports financial support was provided by Business Finland. Zaiqing Que reports financial support was provided by Business Finland. Leena Hupa reports financial support was provided by Business Finland. Elina Huttunen-Saarivirta reports financial support was provided by Business Finland. Mari Lindgren reports financial support was provided by Business Finland. If there are other authors, they declare that they have no known competing financial interests or personal relationships that could have appeared to influence the work reported in this paper.

Acknowledgements

The authors would like to thank Professor Timo Saarinen for carrying out the μ-XRF measurements. The research has been funded by Business Finland, Åbo Akademi, VTT Technical Research Centre of Finland Ltd, and Metso via the TOCANEM project (Register numbers 41752/31/2020 for Åbo Akademi, 36409/31/2020 for VTT Technical Research Centre of Finland Ltd, and 40513/31/2020 for Metso). The financial support is acknowledged. This work has been carried out partly within the Research Council of Finland project "Initiation and propagation of high-temperature corrosion reactions in complex oxygen-containing environments" (Decision no. 348963).

References

[1] F.K. Crundwell, M.S. Moats, V. Ramachandran, T.G. Robinson, W.G. Davenport, Extractive Metallurgy of Nickel, Cobalt and Platinum-Group Metals, Elsevier, Oxford, UK, 2011, p. 610.

[2] A. Malfliet, S. Loftian, L. Scheunis, V. Petkov, L. Pandelaers, P.T. Jones, B. Blanpain, Degradation mechanisms and use of refractory linings in copper production processes: a critical review, J. Eur. Ceram. Soc. 34 (2014) 849–876, https://doi.org/10.1016/j.jeurceramsoc.2013.10.005.

[3] W.E. Lee, S. Zhang, Melt corrosion of oxide and oxide-carbon refractories, Int. Mater. Rev. 44 (1999) 77–104, https://doi.org/10.1179/095066099101528234.

[4] I.V. Kojo, A. Jokilaakso, P. Hanniala, Flash smelting and converting furnaces: a 50 Year retrospect, J. Occup. Med. 52 (2000) 57–61, https://doi.org/10.1007/s11837-000-0049-5.

[5] M.E. Schlesinger, Refractories for copper production, Miner. Process. Extr. Metall. Rev. 16 (1996) 125–146, https://doi.org/10.1080/08827509608914131.

[6] I. Pérez, I. Moreno-Ventas, R. Parra, G. Ríos, Post-mortem study of magnesia-chromite refractory used in the gas area of a Submerged Arc Furnace for the copper-making process, Bol. Soc. Espanola Ceram. Vidr. 58 (4) (2019) 178–188, https://doi.org/10.1016/j.bsecv.2018.12.001.

[7] T. Ranki-Kilpinen, E.J. Peuraniemi, M. Mäkinen, in: Sulfide Smelting 2002, TMS, Warrendale, 2002, pp. 261–272.

[8] F.K. Crundwell, M.S. Moats, V. Ramachandran, T.G. Robinson, W.G. Davenport, Extractive Metallurgy of Nickel, Cobalt and Platinum Group Metals, Elsevier, 2011, p. 610, https://doi.org/10.1016/C2009-0-63541-8.

[9] J. Lehmusto, E. Vainio, T. Laurén, M. Lindgren, The effect of deposit temperature on the catalytic SO_2-to-SO_3 conversion in a copper flash smelting heat recovery boiler, Metall. Mater. Trans. B 49 (1) (2018) 434–439, https://doi.org/10.1007/s11663-017-1130-6.

[10] A. Gerle, J. Piotrowski, J. Podwórny, The Influence of order in the cation sublattice of $MgAl_2O_4$, $MgCr_2O_4$ and $MgFe_2O_4$ spinels on the kinetics of topochemical reactions with sulphur oxides, J. Ceram. Sci. Technol. 8 (2) (2017) 183–192, https://doi.org/10.4416/JCST2016-00077.

[11] J.-L. Liow, P. Tsirikis, N.B. Gray, Study of refractory wear in the tuyere region of a Peirce-Smith nickel convertor, Can. Metall. Q. 37 (1998) 99–117, https://doi.org/10.1016/S0008-4433(98)00003-2.

[12] N.Z. Fotoyi, R.H. Eric, Interaction of MgO-MgR_2O_4(R: Al, Cr, Fe) Refractories with SO_2-Containing Gases in Southern African Pyrometallurgy 2011, Edited by R.T. Jones & P. den Hoed, Southern African Institute of Mining and Metallurgy, Johannesburg, 6–9 March 2011.

[13] D. Gregurek, J. Schmidl, A. Spanring, Refractory challenges in nickel and cobalt processing furnaces in Ni-Co 2021: the 5th international symposium on nickel and cobalt. The Minerals, Metals & Materials Series, Springer, Cham, 2021, https://doi.org/10.1007/978-3-030-65647-8_21.

[14] A. Gerle, J. Podwórny, J. Wojsa, W. Zelik, High temperature gaseous corrosion resistance of MgO-containing refractories – a comparative study, Ceram. Int. 42 (2016) 15805–15810, https://doi.org/10.1016/j.ceramint.2016.07.047.

[15] Collaboration: authors and editors of the volumes III/17B-22A-41B. Magnesium oxide (MgO) Debye temperature, heat capacity, density, melting and boiling points, hardness. In: Madelung, O., Rössler, U., Schulz, M. (eds) II-VI and I-VII Compounds; Semimagnetic Compounds. Landolt-Börnstein - Group III Condensed Matter, vol 41B. Springer, Berlin, Heidelberg.

[16] PAULING FILE in: inorganic solid phases, SpringerMaterials (online database), in: P. Villars (Ed.), SpringerMaterials, $MgCr_2O_4$ Crystal Structure Sd_1510220 (Springer-Verlag GmbH, Heidelberg, © 2016, Springer, Heidelberg, 2005, pp. 309–314, https://doi.org/10.1007/s11148-006-0003-3. M. S. Fedorov, L. N. Ertseva, L. B. Tsymbulov, Corrosive interaction between slags high in copper and nickel oxides and periclase, periclase-chromite, and chromite refractories. Refractories and Industrial Ceramics 46.

[17] M.S. Fedorov, L.N. Ertseva, L.B. Tsymbulov, Corrosive interaction between slags high in copper and nickel oxides and periclase, periclase-chromite, and chromite refractories, Refract. Ind. Ceram. 46 (2005) 309–314, https://doi.org/10.1007/s11148-006-0003-3.

[18] P. Taskinen, A. Jokilaakso, Reaction sequences in flash smelting and converting furnaces: an in-depth view, Metall. Mater. Trans. B 52 (2021) 3524–3542, https://doi.org/10.1007/s11663-021-02283-7.

[19] J. Lehmusto, D. Stenlund, M. Lindgren, P. Yrjas, P, Deposit build-up and corrosion in a copper flash smelting heat recovery boiler, Oxid. Metals 87 (1–2) (2017) 199–214, https://doi.org/10.1007/s11085-016-9666-4.

[20] E. Tomaszewicz, M. Kotfica, Mechanism and kinetics of thermal decomposition of nickel(II) sulfate(VI) hexahydrate, J. Therm. Anal. Calorim. 77 (2004) 25–31, https://doi.org/10.1023/B:JTAN.0000033184.32714.7f.

[21] P. Masset, J.-Y. Poinso, J.-C. Poignet, TG/DTA/MS Study of the thermal decomposition of $FeSO_4{\cdot}6H_2O$, J. Therm. Anal. Calorim. 83 (2006) 457–462, https://doi.org/10.1007/s10973-005-7267-6.

[22] H. Zargar, G. Oprea, T. Troczynski, Influence of solid solution formation on the solid state sintering of $MgCr_2O_4$. Proceedings of the Unified International Technical Conference on Refractories UNITECR2013, pp. 313-317. https://doi.org/10.1002/9781118837009.ch55.

[23] T.I. Shchekina, E.N. Gramenitskii, A.M. Batanova, YaO. Alfer'eva, A.A. Sokolov, R. A. Trofimenko, A.N. Pyrikov, B.N. Grigor'ev, A.V. Likhodievskii, T.N. Us, Phase formation processes and structural changes in chromite-periclase refractories used during nickel production, Refract. Ind. Ceram. 52 (5) (2012) 363–376, https://doi.org/10.1007/s11148-012-9433-2.

[24] V. Petkov, P.T. Jones, E. Boydens, B. Blanpain, P. Wollants, Chemical corrosion mechanisms of magnesia-chromite and chrome-free refractory bricks by copper metal and anode slag, J. Eur. Ceram. Soc. 27 (6) (2007) 2433–2444, https://doi.org/10.1016/j.jeurceramsoc.2006.08.020.

[25] L. Scheunis, M. Campforts, P.T. Jones, B. Blanpain, A. Malfliet, The influence of slag compositional changes on the chemical degradation of magnesia-chromite refractories exposed to PbO-based non-ferrous slag saturated in spinel, J. Eur. Ceram. Soc. 35 (1) (2015) 347–355, https://doi.org/10.1016/j.jeurceramsoc.2014.08.017.

[26] L. Scheunis, A. Fallah-Mehrjardi, M. Campforts, P.T. Jones, B. Blanpain, A. Malfliet, E. Jak, The effect of a temperature gradient on the phase formation inside a magnesia-chromite refractory in contact with a non-ferrous PbO-SiO_2-MgO slag, J. Eur. Ceram. Soc. 35 (10) (2015) 2933–2942, https://doi.org/10.1016/j.jeurceramsoc.2015.03.028.

[27] L. Scheunis, A. Fallah-Mehrjardi, M. Campforts, P.T. Jones, B. Blanpain, E. Jak, The effect of phase formation during use on the chemical corrosion of magnesia-chromite refractories in contact with a non-ferrous PbO-SiO_2 based slag, J. Eur. Ceram. Soc. 34 (6) (2014) 1599–1610, https://doi.org/10.1016/j.jeurceramsoc.2013.12.026.

[28] L. Xu, M. Chen, N. Wang, S. Gao, Chemical wear mechanism of magnesia-chromite refractory for an oxygen bottom-blown copper smelting furnace: a post-mortem analysis, Ceram. Int. 47 (2021) 2908–2915, https://doi.org/10.1016/j.ceramint.2020.09.124.

[29] M. Ludwig, E. Śnieżek, I. Jastrzębska, A. Piwowarczyk, A. Wojteczko, Y. Li, J. Szczerba, Corrosion of magnesia-chromite refractory by PbO-rich copper slags, Corrosion Sci. 195 (2022) 109949, https://doi.org/10.1016/j.corsci.2021.109949.

[30] I. Jastrzębska, M. Ludwig, E. Śnieżek, A. Kalęba, P. Drożdż, J. Szczerba, Corrosion study of novel Cr-free alumina-spinel refractory material dedicated to the copper industry, J. Eur. Ceram. Soc. 42 (15) (2022) 7311–7327, https://doi.org/10.1016/j.jeurceramsoc.2022.08.038.

[31] F.P. Glasser, L.S. Dent Glasser, Crystal chemistry of some AB_2O_4 compounds, J. Am. Ceram. Soc. 46 (8) (1963) 377–380, https://doi.org/10.1111/j.1151-2916.1963.tb11755.x.

[32] J. Podwórny, J. Piotrowski, J. Wojsa, Investigations into the kinetics and mechanism of gas–solid state processes in MgO–MgR_2O_4 (R: Al, Cr, Fe) spinels–SO_2–O_2 system, Ceram. Int. 34 (2008) 1587–1593, https://doi.org/10.1016/j.ceramint.2007.04.019.
[33] A. Gerle, J. Piotrowski, J. Podwórnya, Kinetics of the topochemical reaction of the solid solutions of magnesia spinels: $Mg(Cr_{0.5}Fe_{0.5})_2O_4$, $Mg(Al_{0.5}Cr_{0.5})_2O_4$, $Mg(Al_{0.5}Fe_{0.5})_2O_4$ with sulphur oxides, Thermochim. Acta 680 (2019) 178344, https://doi.org/10.1016/j.tca.2019.178344.
[34] A. Gerle, J. Piotrowski, J. Podwórny, Thermochemistry of $MgCr_2O_4$, $MgAl_2O_4$, $MgFe_2O_4$ spinels in $SO_2-O_2-SO_3$ atmosphere, Processing and Application of Ceramics 10 (1) (2016) 25–31, https://doi.org/10.2298/PAC1601025G.
[35] D.M. Fonseca, D. Gregurek, E.H.M. Nunes, Application of a novel and simple TEST to evaluate the corrosion resistance of magnesia-based refractories to sulfur gases, Ceram. Int. 46 (2020) 26160–26167, https://doi.org/10.1016/j.ceramint.2020.07.113.
[36] J. Lehmusto, T. Laurén, M. Lindgren, The catalytic role of process dust in the SO_2-to-SO_3 conversion in flash smelting heat recovery boilers, J. Occup. Med. 71 (9) (2019) 3305–3313, https://doi.org/10.1007/s11837-019-03464-1.
[37] K. Wieczorek-Ciurowa, Catalytic sulphation of limestone/lime with platinum, J. Therm. Anal. 38 (1992) 2101–2107, https://doi.org/10.1007/BF01979622.
[38] M.N. Scheidema, P. Taskinen, Decomposition thermodynamics of magnesium sulfate, Ind. Eng. Chem. Res. 50 (2011) 9550–9556, https://doi.org/10.1021/ie102554f.
[39] D. Kocaefe, D. Karman, F.R. Steward, Comparison of the sulfation rates of calcium, magnesium and zinc oxides with SO_2 and SO_3, Can. J. Chem. Eng. 63 (6) (1985) 971–977, https://doi.org/10.1002/cjce.5450630614.
[40] D. Kocaefe, D. Karman, F.R. Steward, Interpretation of the sulfation rate of CaO, MgO, and ZnO with SO_2 and SO_3, AIChE J. 33 (11) (1987) 1835–1843, https://doi.org/10.1002/aic.690331110.
[41] S.-M. Shih, J.-C. Lai, C.-H. Yang, Kinetics of the reaction of dense CaO particles with SO_2, Ind. Eng. Chem. Res. 50 (2011) 12409–12420, https://doi.org/10.1021/ie2009668.
[42] C. Hsia, G.R. St Pierre, K. Raghunathan, L.-S. Fan, Diffusion through $CaSO_4$ formed during the reaction of CaO with SO_2 and O_2, AIChE J. 39 (1993) 698–700, https://doi.org/10.1002/aic.690390419.
[43] C. Hsia, G.R. St Pierre, L.-S. Fan, Isotope study on diffusion in $CaSO_4$ formed during sorbent-flue-gas reaction, AIChE J. 41 (1995) 2338–2340, https://doi.org/10.1002/aic.690411020.
[44] L. Chen, S. Li, P.T. Jones, M. Guo, B. Blanpain, A. Malfliet, Identification of magnesia-chromite refractory degradation mechanisms of secondary smelter linings, J. Eur. Ceram. Soc. 36 (2016) 2119–2132, https://doi.org/10.1016/j.jeurceramsoc.2016.02.036.
[45] Z. Yu, Z. Liu, F. Ye, L. Xia, Corrosion mechanism of magnesia-chrome and alumina-chrome refractories in E-scrap smelting, Ceram. Int. 48 (2022) 2693–2703, https://doi.org/10.1016/j.ceramint.2021.10.054.
[46] W. Liu, L. Wang, B. Ma, C. Wang, F. Liu, Y. Chen, Reactions between magnesia-chrome refractories and copper converter slags: corrosion behaviour and prevention by Fe-rich layer formation, Ceram. Int. 48 (2022) 14813–14824, https://doi.org/10.1016/j.ceramint.2022.02.018.